Biophysical Journal, Volume *115*

Supplemental Information

Quantifying Platelet Margination in Diabetic Blood Flow

Hung-Yu Chang, Alireza Yazdani, Xuejin Li, Konstantinos A.A. Douglas, Christos S. Mantzoros, and George Em Karniadakis

Supplementary Materials:

Quantifying Platelet Margination in Diabetic Blood Flow

H.-Y. Chang[1], A. Yazdani[1], X. J. Li[1], K. A. A. Douglas[2,3], C. S. Mantzoros[3], and G. E. Karniadakis[1,*]

[1] Division of Applied Mathematics, Brown University, Providence, RI 02912, U.S.A.
[2] S. Lepida Biomedical Laboratory, Athens 11146, Greece
[3] Division of Endocrinology, Diabetes and Metabolism, Beth Israel Deaconess Medical Center, Harvard Medical School, Boston, MA 02215, USA.
E-mail: George_Karniadakis@brown.edu.

Appendix A. Hydrodynamics and cell models

We employ dissipative particle dynamics (DPD) to model whole blood flow, *i.e.* plasma, red blood cells (RBCs), platelets and white blood cells (WBCs) in the microfluidic channels. The DPD method is a mesoscopic particle-based simulation technique, where each DPD particle represents a lump of molecules and interacts with other particles through soft pairwise forces. Since these interactions depend only on the relative positions and velocities, the resulting DPD fluids are Galilean invariant. Therefore, DPD can provide the correct hydrodynamic behavior of fluids at the mesoscale, and it has been successfully applied to study complex fluids (1, 2). The equation of motion for each particle i is governed by the sum of pair interactions $\mathbf{f}_i$ with the surrounding particles j and integrated using a velocity-Verlet algorithm. The time evolution of velocity ($\mathbf{v}_i$) and position ($\mathbf{r}_i$) of a particle i with mass m_i is determined by Newton's second law of motion:

$$\mathrm{d}\mathbf{r}_i = \mathbf{v}_i \,\mathrm{d}t\,; \quad \mathrm{d}\mathbf{v}_i = \mathbf{f}_i/m_i \,\mathrm{d}t. \tag{1}$$

In the classical DPD method, the total force $\mathbf{f}_i$ exerted on particle i by particle j is composed of a conservative force ($\mathbf{F}_{ij}^C$), a dissipative force ($\mathbf{F}_{ij}^D$), and a random force ($\mathbf{F}_{ij}^R$) given by

$$\mathbf{F}_{ij}^C = a_{ij}(1-\frac{r_{ij}}{r_c})\hat{\mathbf{r}}_{ij} \quad for \quad r_{ij} \le r_c; \quad 0 \quad for \quad r_{ij} > r_c, \tag{2}$$

$$\mathbf{F}_{ij}^D = \gamma\omega_d(r_{ij})(\hat{\mathbf{r}}_{ij}\cdot\hat{\mathbf{v}}_{ij})\hat{\mathbf{r}}_{ij}, \tag{3}$$

$$\mathbf{F}_{ij}^R = \sigma\omega_r(r_{ij})\frac{\zeta_{ij}}{\sqrt{dt}}\hat{\mathbf{r}}_{ij}, \tag{4}$$

where r_c is a cut-off radius, and a_{ij}, γ, σ are the conservative, dissipative and random coefficients, respectively, r_{ij} is the distance with the corresponding unit vector $\hat{\mathbf{r}}_{ij}$, $\hat{\mathbf{v}}_{ij}$ is the difference between the two velocities, ζ_{ij} is a Gaussian random number with zero mean and unit variance, and dt is the simulation timestep size. The parameters γ and σ and the weight functions coupled through the fluctuation-dissipation theorem and are related by $\omega_d = \omega_r^2$ and $\sigma^2 = 2\gamma k_B T$, where k_B is the Boltzmann constant and T is the temperature of the system. The weight function $\omega_r(r_{ij}) = (1-r_{ij}/r_c)^k$ with $k = 1$ in the standard DPD method, whereas other values of k have been used to increase the fluid viscosity (3). More detailed description of DPD method can be found elsewhere (4, 5); see also (6) for RBC and platelet modeling.

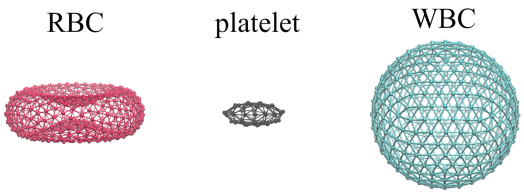

Figure S1: Schematic of the RBC, platelet, and WBC models.

In addition to blood plasma modeled by collections of free DPD particles, the membrane of suspending cells including RBCs, platelets, and WBCs is constructed by a 2D triangulated network with N_v vertices (DPD particles). The vertices are connected by N_s elastic bonds to impose proper membrane mechanics, see the schematic cell models in Fig. S1. This DPD representation of RBCs, platelets, and WBCs was extensively used and validated in the previous studies for both healthy and diseased cells (6–9). For a single cell, the free energy (V_{cell}) is given by

$$V_{cell} = V_s + V_b + V_{a+v}. \tag{5}$$

The elastic energy V_s representing the elastic interactions of the cell membrane is defined by

$$V_s = \sum_{j \in 1 \dots N_s} \left[\frac{k_{\mathrm{B}} T l_m (3x_j^2 - 2x_j^3)}{4p(1 - x_j)} + \frac{k_p}{l_j} \right], \tag{6}$$

where p is the persistence length, k_p is the spring constant, $k_{\mathrm{B}}T$ is the energy unit, l_j is the length of the spring j, l_m is the maximum spring extension, and $x_j = l_j/l_m$. p and k_p are computed by balancing the forces at equilibrium and from their relation to the macroscopic shear modulus, μ_s:

$$\mu_s = \frac{\sqrt{3} k_{\mathrm{B}} T}{4 p l_m x_0} \left(\frac{x_0}{2(1 - x_0)^3} - \frac{1}{4(1 - x_0)^2} + \frac{1}{4} \right) + \frac{3\sqrt{3} k_p}{4 l_0^3}, \tag{7}$$

where l_0 is the equilibrium spring length and $x_0 = l_0/l_m$. The bending resistance V_b of the cell membrane is modeled by

$$V_b = \sum_{j \in 1 \dots N_s} k_b \left[1 - cos(\theta_j - \theta_0) \right], \tag{8}$$

where k_b is the bending constant, and it is related to the macroscopic bending rigidity k_c with the expression $k_b = 2k_c/\sqrt{3}$, θ_j is the instantaneous angle between two adjacent triangles having the common edge j, and θ_0 is the spontaneous angle. In addition, the area and volume constraints V_{a+v} are imposed to mimic the area-preserving lipid bilayer and the incompressible interior fluid. The corresponding energy is given by

$$V_{a+v} = \sum_{j \in 1 \dots N_t} \frac{k_d (A_j - A_0)^2}{2A_0} + \frac{k_a (A_{\text{cell}} - A_0^{\text{tot}})^2}{2A_0^{\text{tot}}} + \frac{k_v (V_{\text{cell}} - V_0^{\text{tot}})^2}{2V_0^{\text{tot}}}, \tag{9}$$

where N_t is the number of triangles in the membrane network, A_0 is the equilibrium value of a triangle area, and k_d, k_a and k_v are the local area, global area and volume constraint coefficients, respectively. The terms A_0^{tot} and V_0^{tot} are targeted cell area and volume. In practice, we use high values for the constraint coefficients to enforce area and volume incompressibility.

Fluid-cell interactions are achieved through viscous friction using the dissipative and random DPD forces. In order to impose appropriate boundary conditions between the fluid and the cell membrane, a DPD dissipative force ($\mathbf{F}^D$) between fluid particles and membrane vertices needs to be properly applied. The dissipative coefficient γ is computed such that no-slip condition on cell surface is enforced and γ is derived based on the idealized case of linear shear flow over a patch of RBC membrane. The total shear force exerted by the fluid on a patch of area A is equal to $A\eta\dot{\gamma}$, where η is the viscosity of fluid and $\dot{\gamma}$ is the local wall shear rate.

In DPD discrete form, we distribute a number of particles on the wall to mimic the membrane vertices. The force (F_v) on a single wall particle exerted by the fluid can be found as follows

$$F_v = \int_{V_H} ng(r)\mathbf{F}^D \mathrm{d}V\,, \tag{10}$$

where n is the fluid number density, $g(r)$ is the radial distribution function of fluid particles with respect to the wall particles, and V_H is the half sphere volume of fluid above the wall. The total shear force on the area A is equal to $F_v N_A$, where N_A is the number of wall particles on the patch with area A. The radial distribution function is uniform $g(r) = 1$ when the repulsive conservative interaction between fluid and wall particles is zero (6, 10). The repulsive-force coefficient for the fluid-cell interactions is therefore set to zero, and the dissipative coefficients can be computed through the equality of $F_v N_A = A\eta\dot{\gamma}$. The DPD parameters used in eqn (2)-(4) for all types of DPD particles and the cell membrane parameters used in eqn (6)-(9) for all blood cell models are given in Tables S1 and S2, respectively.

Table S1: DPD parameters used in simulations. r_c is the cut-off radius, a_{ij} is the conservative coefficient, γ is the dissipative coefficient, and k is the weight function exponent. In all simulations, we set the particle mass $m = 1$, and the thermal energy $k_B T = 0.10$ in DPD units. Note that S= solvent (representing plasma), R= RBC, P= platelet, and W= WBC.

type	r_c	a_{ij}	γ	k
S-S	1.58	5.0	20.0	0.20
S-R	1.5	0.0	45.0	0.20
S-P/S-W	1.5	0.0	10.0	0.20
R-R	1.0	10.0	10.0	0.20
R-P/R-W	1.0	10.0	10.0	0.20
P-P/P-W/W-W	1.0	10.0	10.0	0.20

In order to prevent cell overlap we also adopt a Morse potential between cell membrane particles in the form of

$$V_M(r) = D_e[e^{2\beta(r_0-r)} - 2e^{\beta(r_0-r)}]\,, \tag{11}$$

where r is the separation distance, r_0 is the zero force distance, D_e is the well depth of the potential, and β characterizes the interaction range. By properly setting the parameters, we can ensure strong repulsive forces between cell membrane particles and prevent their overlap. We present the Morse potential parameters used for cell-cell interactions in Table S3. Note that the cutoff radius $r_{cM} = 1$ is set for all the Morse interactions.

It is also important to derive the scaling relationships between model (DPD) units and physical units. We first define the length scale as

$$r^M = \frac{D_0^P}{D_0^M}\,, \tag{12}$$

where D_0 is the RBC diameter, r^M is the model unit of length, and the superscripts M and P denote the model and physical units, respectively. In the current study, we consider D_0^P = 7.82$\times 10^{-6}$ m (11), D_0^M = 7.82, then r^M = 1.0$\times 10^{-6}$ m can be obtained. In addition, the time scale is defined as

$$\tau = \frac{D_0^P}{D_0^M}\frac{\eta^P}{\eta^M}\frac{\mu_0^M}{\mu_0^P}\,, \tag{13}$$

Table S2: Cell membrane parameters for normal RBCs (NRBCs), diabetic RBCs (DRBCs), platelets with mean platelet volume (MPV)= 6 fL (PLTs), platelets with MPV= 12 fL (PLT*), and white blood cells (WBCs). N_v is the number of DPD particles on the membrane, l_m is the maximum bond extension, l_0 is the equilibrium bond length, k_b is the bending constant, μ_s is the shear modulus, A_0^{tot} and V_0^{tot} are the specified cell area and volume, respectively, $k_d + k_a$ is the combined area constraint coefficient, and k_v is the volume constraint coefficient.

cell	N_v	l_m/l_0	k_b	μ_s	A_0^{tot} (V_0^{tot})	$k_d + k_a$ (k_v)
NRBC	500	1.8	6.025	100.0	132.87 (92.45)	5000 (5000)
DRBC	500	1.8	6.025	200.0	132.87 (127.45)	5000 (5000)
PLT	48	1.8	100.0	10^4	19.63 (6.02)	5000 (10^4)
PLT*	48	1.8	100.0	10^4	31.16 (12.01)	5000 (10^4)
WBC	2498	1.8	6.025	2200.0	313.78 (522.44)	50000 (5×10^4)

Table S3: Morse potential parameters for cell-cell interactions. D_e is the well depth of the potential, r_0 is the zero force distance, and β characterizes the interaction range. Note that R= RBC, P= platelet, and W= WBC.

type	D_e	β	r_0
R-R	5.0	2.0	0.95
R-P/R-W	10.0	2.0	1.0
P-P/P-W/W-W	10.0	2.0	1.0

where η is the viscosity of plasma and μ_0 is the RBC shear modulus. In this study, we consider η^P = 1.25×10^{-3} Pa·s, μ_0^P = 4.73×10^{-6} N/m, η^M= 148 and μ_0^M = 100 (6, 12, 13), then the DPD time scale is τ = 1.8×10^{-4} s. The size of a DPD particle for representing blood plasma can be estimated by

$$V_{dpd} = V_D/N_l\,, \tag{14}$$

where we used the volume of the modeled domain V_D = 113411.5 μm^3 and the number of solvent particles in the domain N_l= 365014. Hence, a particle size is V_{dpd} = 3.1×10^{-19} m^3. The volume of a water molecule is $\sim3\times10^{-29}$ m^3 (14). Therefore, the mapping between the water molecules and a solvent bead in our system is at the scale of $\mathcal{O}(10^{10})$ water molecules/DPD particle.

Appendix B. DPD model validation

The focus of this study is quantifying platelet margination in diabetic blood flow via a high-fidelity numerical approach. It is important to validate the numerical model prior to using it in applications extensively. As there is little to no available microfluidic data on platelet margination in the literature, we resort to the measurements made for marginated polystyrene micro-beads suspended in bovine blood from the work of Carboni *et al.* (15).

In order to have the closest possible comparison with the experimental measurements, a rectangular channel with the same height ($40\ \mu m$) is considered in our DPD simulations with human blood driven by the pressure gradient, which generates different flowrates corresponding to wall shear rates of 60 and 120 s^{-1} similar to the experiment. The width of the channel is assumed to be much larger than its height, which makes

the DPD system periodic along the width of the channel. Further, we assume a periodic channel flow along the flow direction. Rigid spherical particles of variable sizes, 0.53, 0.84 and 2.11 μm, are modeled by DPD particles connected to each other through stiff wormlike chains (WLCs) (16) similar to the model described for platelets. For smaller beads, however, 12 DPD particles are used to form the sphere, as opposed to 42 DPD particles used for the largest bead.

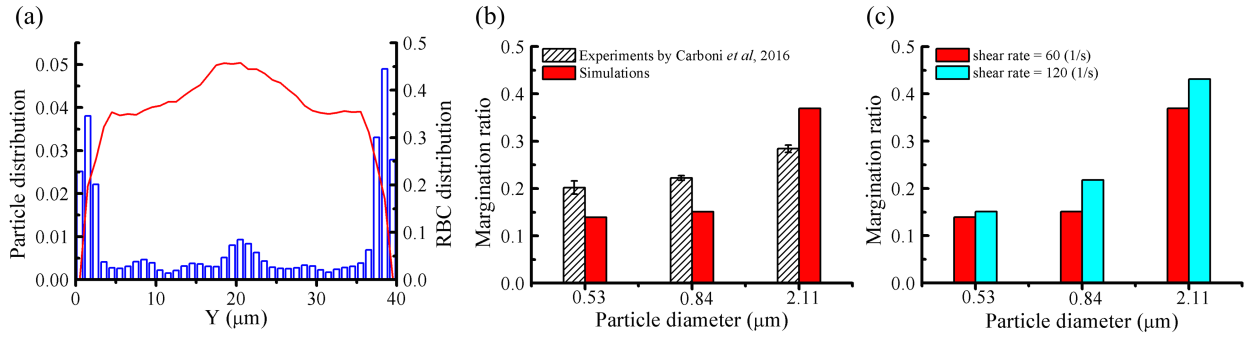

Figure S2: DPD model validation and comparison with microfluidic measurements for rigid spherical particles. (a) Time-averaged particle (bars) and RBC volume fraction (red line) along the channel height (particle diameter 2.11 μm). (b) Comparison of computed and measured margination ratios for spherical particles of different sizes, with experimental data by Carboni *et al.* (15). (c) Computed margination ratios for different particle sizes evaluated for two wall shear rates.

A representative result for time-averaged particle and RBC distributions across the channel height is given in Fig. S2, where both distributions are given as volume fractions. The mean volume fraction of RBCs is 35% (blood hematocrit used in experiments (15)), a rise in RBC volume fraction close to the center of the channel and the depletion of RBCs adjacent to the channel walls are clear. The cell free layer (CFL) thickness is estimated to be $\approx 2\mu m$, which is used for calculating the margination ratio. The spherical particles volume fraction is quite higher in the CFL due to the margination effects.

Margination ratio (referred to as *margination percentage* in the main text) defined as the ratio of marginated particles in the CFL divided by the number of suspended particles is plotted in Fig. S2(b) for three different particle sizes at wall shear rate 60 s^{-1}. The results show good comparison with the experiments, suggesting that the margination ratio increases by the size of the particles. The difference, however, could be attributed to the image resolution in the experiments and the fact that bin sizes considered in the experiment are relatively larger than the CFL thickness. It is also noted that the different sizes of RBCs adopted in the experiment (15) and simulation (bovine RBCs with diameter 5-6 μm (17) vs. human RBCs with diameter 7.5-8.7 μm (11)) could lead to slight differences in the magnitude of margination ratio in our simulations. However, the simulation results will not be affected qualitatively because we keep the blood hematocrit (H_{ct}= 35%) the same as the experiments (15). The volume fraction of RBCs is detrimental in the frequency of particle collisions with the RBCs that leads to particle margination (18, 19). In addition, the effect of shear rate on particles margination is plotted in Fig. S2(c). Increasing the shear rate enhances particle margination (which is observed for oblate platelets as well) for all particle sizes as reported by the experiment of Carboni *et al.* (15), and confirmed in a few other numerical simulations (6, 20). In the current model validation, we only consider particles with spherical shapes and not the oblate spheroids (the shape of a resting platelet) since spherical polystyrene micro-beads were used in the experiment. In fact, particle shapes are also important for margination, which have been investigated numerically in a few other studies. Reasor *et al.* (21) observed that comparing with the spherical particles, the oblate particles (in particular the disk-like oblates) were easily trapped in the center-occupied RBC core, lowering their margination rate. On the other hand, Vahidkhah and Bagchi (22) found that the frequency of particle-RBC collision played a key role in determining particle margination rate, and the oblate particles of moderate aspect ratio (AR=0.5) exhibited the highest frequency among the spherical, rod-like, and oblate particles (AR=0.3,0.5).

Appendix C. Blood sample preparation and analysis procedures

Clinical data from 136 consecutively subjects were pulled from the biochemical database of the S. Lepida Biomedical Laboratory in Athens Greece specifically for this study. Data had been obtained using standard automatic biochemical analyzers (Sysmex XT-1800i and ILAB 350 Clinical Chemistry System) were anonymized and thus exempt from IRB oversight. Clinical data included HbA1c, fasting glucose level, mean corpuscular volume (MCV), mean platelet volume (MPV), plateletcrit (PCT), and WBC counts. A total of 64 type 2 diabetic patients (30 males and 34 females; age, 61$\pm$13.69 years; range, 34 – 90 years) and 72 healthy controls (30 males and 42 females; age, 52$\pm$17.80 years; range, 26 – 94 years) were included in the study, and the clinical data were analyzed by one-way analysis of variance (ANOVA). Variables given as absolute or mean value $\pm$ standard error are shown in Table S4. Statistical significance was defined as $p <$0.05.

As shown in Table S4 and Fig. S3, despite the slightly decreased mean value of MCV in diabetic subjects, $p =$0.05 estimated based on one-way ANOVA test indicates no significant difference in MCV of control and diabetic blood samples. On the other hand, there are significantly higher MPV (10.0$\pm$1.26 fL vs 9.2$\pm$1.70 fL, $p =$0.003), PCT (0.23$\pm$0.06 % vs 0.21$\pm$0.07 %, $p =$0.02), and WBC count (8.04$\pm$2.16 k/μL vs 6.85$\pm$1.96 k/μL, $p =$0.001) for diabetic subjects compared with non-diabetics.

Table S4: Clinical characteristics of the study groups

	Controls	Diabetics	p-value
Total subject number	72	64	–
Male/ Female	30/ 42	30/ 34	–
Age range (years)	26 – 94	34 – 90	–
Mean age (years)	52 $\pm$ 17.80	61 $\pm$ 13.69	–
Mean HbA1c (%)	5.25 $\pm$ 0.29	7.66 $\pm$ 1.41	–
Fasting glucose (mg/dl)	99.0 $\pm$ 15.4	144.5 $\pm$ 45.8	–
MCV (fL)	88.33 $\pm$ 7.76	85.26 $\pm$ 9.89	0.05
MPV (fL)	9.2 $\pm$ 1.70	10.0 $\pm$ 1.26	0.003
PCT (%)	0.21 $\pm$ 0.07	0.23 $\pm$ 0.06	0.02
WBC count (k/μL)	6.85 $\pm$ 1.96	8.04 $\pm$ 2.16	0.001

Variables are expressed as mean value $\pm$ standard error. Note that MCV= mean corpuscular volume, MPV= mean platelet volume, and PCT= plateletcrit. p-value is estimated based on one-way ANOVA test.

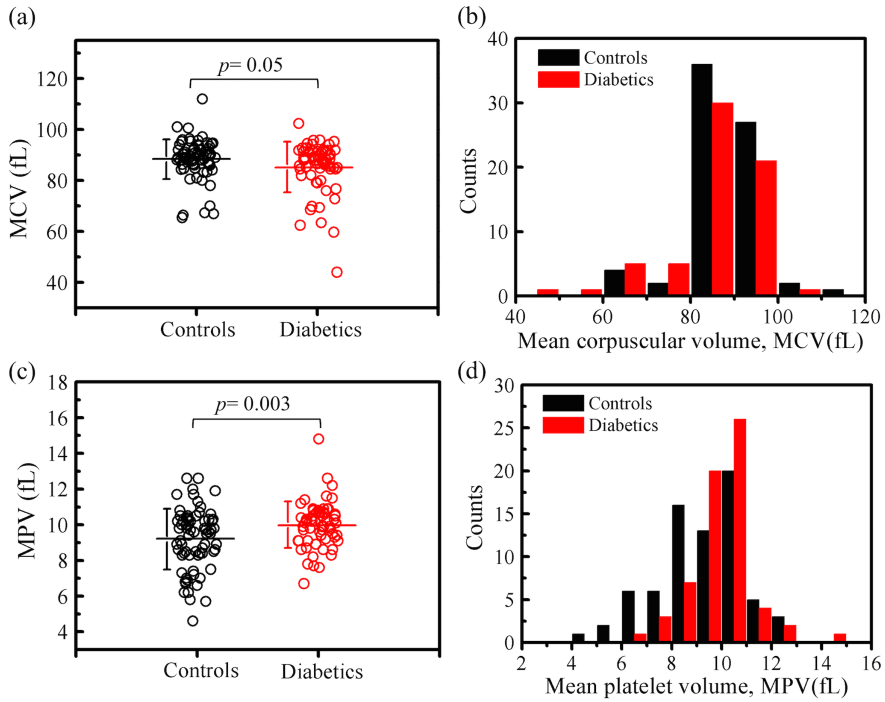

Figure S3: Mean corpuscular volume (MCV) and mean platelet volume (MPV) from healthy controls and diabetic patients. (a) and (c) Scatter plots of all measured data, where the horizontal lines are mean values and the vertical error bars are the sample standard deviation. (b) and (d) Histograms showing the count distributions of MCV and MPV in controls and diabetics.

References

1. Fedosov, D. A., W. Pan, B. Caswell, G. Gompper, and G. E. Karniadakis, 2011. Predicting human blood viscosity in silico. *Proc. Natl. Acad. Sci. U.S.A* 108:11772–11777.

2. Ye, T., N. Phan-Thien, and C. T. Lim, 2016. Particle-based simulations of red blood cells - a review. *J. Biomech.* 49:2255–2266.

3. Fan, X., N. Phan-Thien, S. Chen, X. Wu, and T. Yong Ng, 2006. Simulating flow of DNA suspension using dissipative particle dynamics. *Phys. Fluids* 18:063102.

4. Espanol, P., and P. Warren, 1995. Statistical mechanics of dissipative particle dynamics. *Europhys. Lett.* 30:191.

5. Groot, R. D., and P. B. Warren, 1997. Dissipative particle dynamics: bridging the gap between atomistic and mesoscopic simulation. *J. Chem. Phys.* 107:4423–4435.

6. Yazdani, A., and G. E. Karniadakis, 2016. Sub-cellular modeling of platelet transport in blood flow through microchannels with constriction. *Soft Matter* 12:4339–4351.

7. Fedosov, D. A., B. Caswell, and G. E. Karniadakis, 2010. A multiscale red blood cell model with accurate mechanics, rheology, and dynamics. *Biophys. J.* 98:2215–2225.

8. Pivkin, I. V., and G. E. Karniadakis, 2008. Accurate coarse-grained modeling of red blood cells. *Phys. Rev. Lett.* 101:118105.

9. Lei, H., and G. E. Karniadakis, 2013. Probing vasoocclusion phenomena in sickle cell anemia via mesoscopic simulations. *Proc. Natl. Acad. Sci. U.S.A* 110:11326–11330.

10. Fedosov, D. A., B. Caswell, A. S. Popel, and G. E. Karniadakis, 2010. Blood flow and cell-free layer in microvessels. *Microcirculation* 17:615–628.

11. Diez-Silva, M., M. Dao, J. Han, C.-T. Lim, and S. Suresh, 2010. Shape and biomechanical characteristics of human red blood cells in health and disease. *MRS Bulletin* 35:382–388.

12. Baskurt, O. K., M. R. Hardeman, and M. W. Rampling, 2007. Handbook of hemorheology and hemodynamics, volume 69. IOS press.

13. Hochmuth, R. M., and R. E. Waugh, 1987. Erythrocyte membrane elasticity and viscosity. *Annu. Rev. Physiol.* 49:209–219.

14. Chang, H.-Y., Y.-L. Lin, Y.-J. Sheng, and H.-K. Tsao, 2012. Multilayered polymersome formed by amphiphilic asymmetric macromolecular brushes. *Macromolecules* 45:4778–4789.

15. Carboni, E. J., B. H. Bognet, G. M. Bouchillon, A. L. Kadilak, L. M. Shor, M. D. Ward, and A. W. Ma, 2016. Direct tracking of particles and quantification of margination in blood flow. *Biophys. J.* 111:1487–1495.

16. Marko, J. F., and E. D. Siggia, 1995. Stretching DNA. *Macromolecules* 28:8759–8770.

17. Adili, N., M. Melizi, H. Belabbas, and A. Achouri, 2014. Preliminary study of the influence of red blood cells size on the determinism of the breed in cattle. *Vet. Med. Int.* 2014:429495.

18. Kumar, A., and M. D. Graham, 2012. Margination and segregation in confined flows of blood and other multicomponent suspensions. *Soft Matter* 8:10536–10548.

19. Kumar, A., R. G. H. Rivera, and M. D. Graham, 2014. Flow-induced segregation in confined multicomponent suspensions: effects of particle size and rigidity. *J. Fluid Mech.* 738:423–462.

20. Mehrabadi, M., D. N. Ku, and C. K. Aidun, 2016. Effects of shear rate, confinement, and particle parameters on margination in blood flow. *Phys. Rev. E* 93:023109.

21. Reasor, D. A., M. Mehrabadi, D. N. Ku, and C. K. Aidun, 2013. Determination of critical parameters in platelet margination. *Ann. Biomed. Eng.* 41:238–249.

22. Vahidkhah, K., and P. Bagchi, 2015. Microparticle shape effects on margination, near-wall dynamics and adhesion in a three-dimensional simulation of red blood cell suspension. *Soft Matter* 11:2097–2109.